CHAPTER 2

Target Localization System Comprising Two Antennas*

*Part of this work has been published as:

Vineet Singh, Somak Bhattacharyya, and Pradip Kumar Jain. "Implementation of a simple stepped frequency continuous wave target localization system comprising two antennas based on common region of sensing," *International Journal of RF and Microwave Computer-Aided Engineering*, vol. 29, no. 8, p. e21795, 2019.

CHAPTER 2

Target Localization System Comprising Two Antennas

In previous chapter, the overview of different radar techniques have been discussed which can be utilized to obtain the target information. Wideband and narrowband are the two main types of radar systems which can be used according the type of target associated information. This chapter mainly deals with the application of wide band system in finding the location of the stationary targets.

In this chapter, a two antenna-based localization system is presented, each creating a single independent ranging unit, working on the principle of stepped frequency continuous wave (SFCW) radar. The proposed system exploits the principle of trilateration and suitable for indoor target localization whose antennas are deployed parallel to any single wall of a room with the flexibility of variable antenna separation distance [Ahmad *et al.* (2009), Torres-Solis *et al.* (2010)]. In this scheme, the detected target location is defined in the simple Cartesian coordinate system whose origin can be taken at one of the antenna positions while the other antenna lies somewhere on *x*-axis. As the developed localization scheme constitutes of SFCW system, the system sensitivity is high and the efficient use of energy for data collection could be implemented using low processor speed in the proposed localization system [Jol (2008), Mercuri *et al.* (2012)]. Furthermore, the use of lesser number of antennas facilitates the lesser processing and operating complexity for both free space as well as through the wall localization scheme. The localization is carried out for different possible subregions of the common region of sensing (CROS). The proposed study focuses on the localization efficiency at any available space in the room.

2.1 SFCW Radar with the Laboratory Components

A simplified block diagram of a SFCW system is shown in Figure 2.1(a) which consists of a RF source along with digital signal processing (DSP) capability [Jol (2008)]. The RF source used in a stepped frequency CW radar is a direct digital synthesis (DDS) source. The source frequency is changed stepwise between a start frequency f_0 and a stop frequency f_{N-1} following the equal and linear increments. The radar continuously transmits and the returned signal is formed by the mixing of the received backscattered signal with a portion of the transmitted one. This return signal is digitized at each step and stored. After each complete sweep of N steps, a Fourier transform is performed to convert the data from the frequency domain to the time domain. This is the process of creating the synthesized pulse.

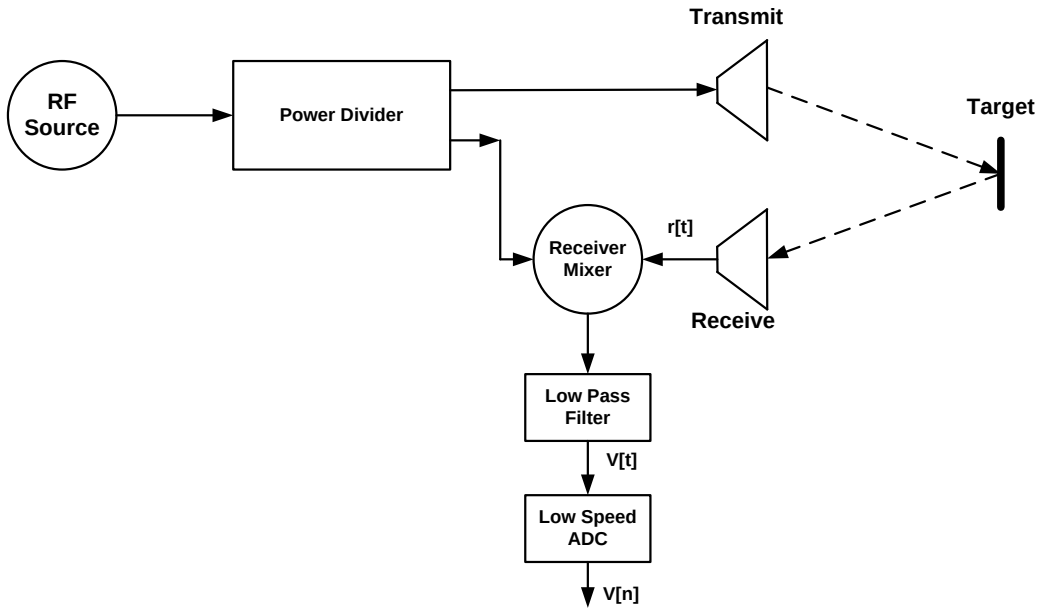

(a)

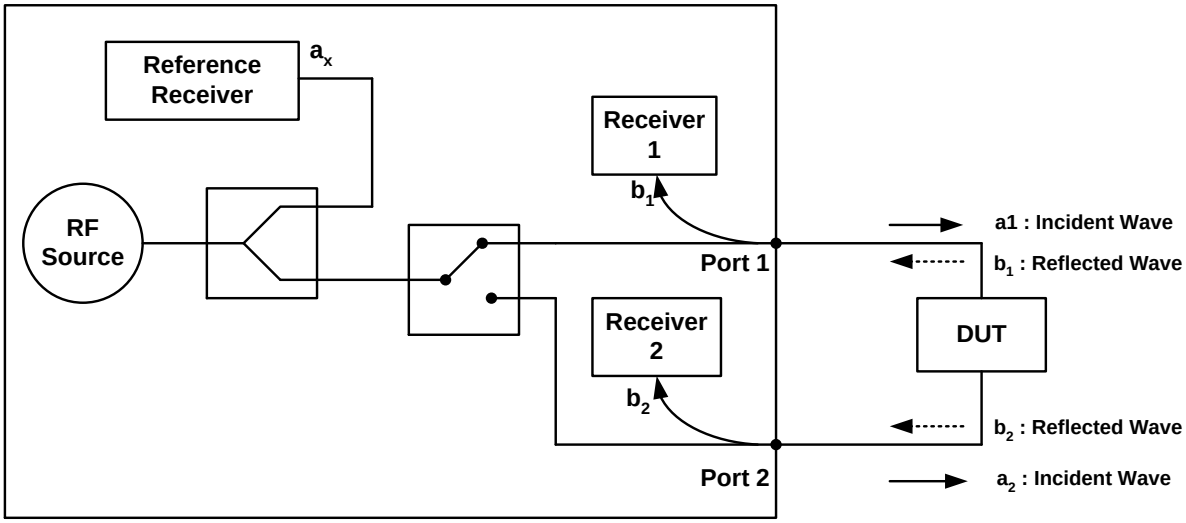

(b)

Figure 2.1: (a) Simplified block diagram of stepped frequency radar; (b) Simplified block diagram of a two-port VNA connected to a DUT.

2.1.1 Vector Network Analyzer

A vector network analyzer (VNA) is quite often used to characterize any high frequency active and passive devices in their linear mode of operation by measuring their S-parameters as a function of frequency. Vector Network analyzer must have the capability to produce wave incident over a wide range of frequencies and amplitudes while separating and measuring the incident and reflected waves across a number of test ports [Yip (2012)]. It is important to know the incident and reflected waves at a specific location for each device under test (DUT) port. Hence it further increases complexity. Figure 2.1(b) is a simplified block diagram of a two-port VNA connected to a DUT. The VNA stimulates the active incident port with a tunable oscillator, which is multiplexed between the two ports with a terminating microwave switch (the unused port is connected to the matched load of 50Ω). The oscillator simultaneously drives both the DUT and a reference receiver (through a power divider) to enable incident wave power measurements. A directional coupler on each port separates reflected waves from incident waves, in which reflected waves are fed to three measurement receivers. All the

three receivers are synchronized in such a way that the relative phase of the wave quantities can be measured directly. The measurement is carried out by sweeping the oscillator between the desired start and stop frequencies while capturing each of the receiver's amplitudes and phases, with one port active at a time. It is important to measure incident and reflected waves at a specific location at each DUT port. This location is known as the reference plane and is critical to successful measurement. The process of setting the reference plane and minimizing error terms is called calibration.

All the required blocks of a SFCW radar systems are present in the VNA along with the desired oscillator and receiver functionalities. Due to this reason for the synthesis of a SFCW system in the laboratory, it is the most suitable choice of researchers in the laboratory [Gaikwad (2011), Amin (2017)].

2.2 SFCW Radar System Range Profile Creation

If the ranging device transmits a continuous wave signal *S(t)* towards a target located at distance *R* and the returned echo received by the device is $S_r(t)$. *S(t)*and $S_r(t)$ can be expressed as:

$$S(t) = A_1 Sin(2\pi f_0 t) \quad , \tag{2.1}$$

and

$$S_r(t) = A_2 Sin(2\pi f_0 t - \varphi) \quad . \tag{2.2}$$

Here, A_1 and A_2 are the amplitudes of the transmitted and returned echo signals, respectively, and $\varphi = (2\pi f_0 \times 2R)/c$ is the phase difference between these two signals where f_0 is the transmitted signal frequency and *c* is the speed of electromagnetic wave in free space [Daniels (2009)]. The phase change $\Delta\varphi$ corresponding to the same range *R* at two different frequencies f_1 and f_2 can be given as:

$$\Delta\varphi = \varphi_2 - \varphi_1 = \frac{4\pi R(f_2 - f_1)}{c} \quad . \tag{2.3}$$

The range R can be maximized when $\Delta\varphi = 2\pi$ which gives rise to the maximum unambiguous range R_{max}:

$$R_{\max} = \frac{c}{2(f_2 - f_1)} \quad . \tag{2.4}$$

If this frequency change is continued over a frequency band following N steps of f_2 - f_1 = Δf size increment, then maximum range can be seen as a combination of downrange resolution and given by:

$$\Delta R = \frac{c}{2(\mathrm{N}-1)\Delta \mathrm{f}} \quad . \tag{2.5}$$

The denominator term of (5) covers the whole bandwidth in which frequency changes are occurring. If the starting point of the frequency band is f_{start} and stop point is f_{stop} then

$$\Delta \mathrm{R} = \frac{\mathrm{c}}{2(f_{stop} - f_{start})} = \frac{\mathrm{c}}{2\mathrm{BW}} \quad . \tag{2.6}$$

From the equations (2.4) and (2.6), it is clear that for the stepped frequency system the maximum range depends on the frequency resolution Δf while minimum detectable range ΔR depends upon the system bandwidth.

From a single sweep data the range profile can be generated, and we can locate the target position in the radar's downrange distance. The frequency domain data collected by VNA can easily be converted into time domain followed by spatial domain translation to achieve the range profile [Chandra *et al.* (2009), Gaikwad *et al.* (2011)]. If z denotes the downrange distance of the target, which is related with signal's round trip travel time t as $z = c \times t/2$ where c is the speed of electromagnetic wave in the air. The spatial domain data $s(z)$ can be expressed in terms of the frequency domain data $s(f_i)$ as:

$$s(z) = \sum_{i=1}^{I} s(f_i) \exp(j 2\pi f_i) 2z / c \ , \quad 0 < z < z_{max}, \tag{2.7}$$

where i^{th} point frequency is f_i and I is the maximum number of the frequency point. Here, f_i is the system's frequency over a single sweep from f_{start} = 8 GHz to f_{stop} = 12 GHz following I (=201) number of steps.

2.2.1 Range Profile Details

The used SFCW system captures the data in frequency domain over a frequency bandwidth of 4 GHZ (8-12 GHz range) while keeping the antenna position fixed. Such type of scanning process is also called A-scan where the RF energy is displayed as a function of time delay or distance from the antenna [Singh and Jain (2016), Benedetto *et al.* (2017)]. The downrange resolution of 3.75 can be computed for the mentioned bandwidth using equation (2.6) while the systems maximum unambiguous range is 7.5 m (equation 2.4).

2.3 Experimental Setup

A two antenna-based object localization system is synthesized here for the experimentation, and its schematic is shown in Figure 2.2. The SFCW radar system is synthesized by connecting the two ports of a Keysight (N9916A) vector network analyzer (VNA) to two pyramidal horn antennas, operating in the X-band. A handheld portable VNA has been used in the experimental setup as it contains all the basic building blocks to constitute an SFCW system [Jol (2008)]. Since a VNA can measure the reflection coefficient at its two ports simultaneously, two transceiver sets can be realized at a time by connecting the antennas on each port. These antennas are mounted such that the distance between them covers the complete wall length and two mono-static systems are created to cover the entire X-band. The VNA based designed system

is able to record the reflection coefficient corresponding to the two antennas in the form of S_{11} and S_{22} simultaneously. To mitigate the effect of the external environment, the entire experimental setup with the scan region is kept within the anechoic chamber [Christopher and Holloway (1997)].

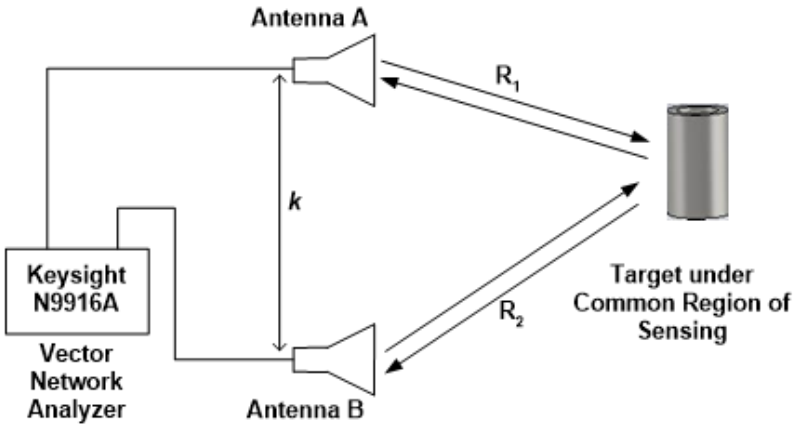

Figure 2.2: Schematic diagram of the experimental setup for target localization within the anechoic chamber.

The downrange resolution of an SFCW radar can be enhanced by increasing the sweep bandwidth of the system [Jol (2008)]. Here the sweep bandwidth of 4 GHz is chosen, where the system begins to sweep from a start frequency of 8 GHz to a stop frequency of 12 GHz following 201 linear incremental frequency steps. For the mentioned sweep setting, a 20 MHz frequency step size is obtained. The VNA calibration is necessary before any measurement, as it removes systematic error and other uncertainties in the DUT measurement effectively. The two port calibration is done over the system's sweep bandwidth at 201 frequency points using the 2-Port SOLT (short-open-load-through) method. The other parameters used in the experiment are summarized in Table 2.1.

Table 2.1: Experimental setup specifications.

Sr. No.	Parameter	Value/specification
1	Antenna Type	X-band horn
2	Source	Keysight analyzer N9916A
3	Frequency Range	8-12 GHz
4	Frequency Step Size	20 MHz
5	Range Resolution	3.75 cm
6	Transmitted Power	−3 dBm
7	Maximum Unambiguous Range	7.5 m
8	Number of Frequency points	201
9	Distance between two antenna positions	1.5 m

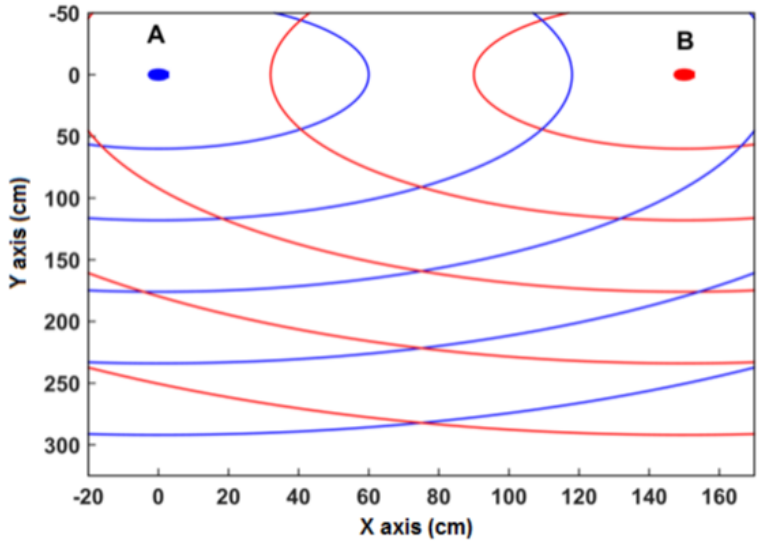

Figure 2.3: Region of sensing for omnidirectional antenna.

2.4 Common Region of Sensing (CROS)

The range estimation procedure of the target from the antenna using SFCW radar is explained in *Section 2.1* in detail. For a two antenna-based system, the complete space available in entire room can be covered by the omnidirectional antenna if the ranging system is mounted on the wall side with proper mutual isolation arrangement. The biggest disadvantage of omnidirectional-based ranging system is that a major portion of

radiated power get wasted due to the radiations in the undesired directions, as shown in Figure 2.3 which drastically reduces the system range and higher power is needed to get the better range coverage [Jol (2008), Daniels (2009), Mahafza and Elsherbeni (2004)].

For two directive antenna-based system, there are some system level electromagnetic constraints on the spatial coverage of the localization system which mainly depends on the antenna beam-width and maximum range of the ranging unit which defines a CROS for two antennas where the placed target can be sensed from both the antennas. The beam width of a horn antenna is different in both directions of a horn antenna with flared opening sides *a* and *b* in horizontal and vertical dimension, respectively, given as [Baltzis (2010)]:

$$\phi_v = 54\lambda / b \quad , \tag{2.8}$$

$$\phi_h = 78\lambda / \mathrm{a} \quad . \tag{2.9}$$

In Figure 2.4, CROS is clearly shown and the covered area, which is basically the overlaps of the radiated beam by the two antennas A and B, is identified within the points OEGDO. The minimum distance ON of the CROS, that is, the starting of the region of sensing from the antenna baseline, depends upon the beam widths of the antenna and the distance between two scan positions *k* and can be written as:

$$D_{\min} = \frac{k}{2\tan(\theta_{BW} / 2)} \quad . \tag{2.10}$$

The other extreme of CROS defined by D_{max} is limited by the maximum range covered by either of the antenna. If the object is lying within CROS, it can be detected by both the antennas as proposed. While if the object is kept outside the CROS, it may be detectable by either of the antenna or may not be detected, depending upon the position of the object.

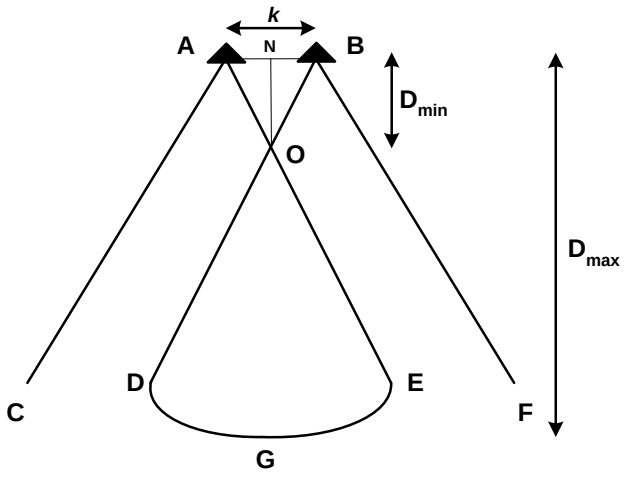

Figure 2.4: Common region of sensing (CROS).

2.4.1 Sub-regions of CROS

If the target is present within the CROS then we will get three possible subregions where the target may be present for a localization problem as illustrated in Figure 2.5. Region 2 is known as the acute angle case where both ranging lines joining the two antennas to the target will make an acute angle with the baseline joining the point of antenna placed at A and B. In this subregion, the coordinate of the target is expressed by equation (2.11).

However, if the target is present in either of the subregions 1 or 3, this will create the obtuse angle case where any of the ranging lines will form an obtuse angle with the baseline joining the two antennas, and their location coordinate is expressed by sub-equation (2.12). Equations (2.11) and (2.12) are valid when the range of the target from antenna A and B, i.e., R_1 and R_2 are known. A function is implemented in MATLAB script to decide the subregion type and to find the location coordinate accordingly.

$$x_0 = \frac{R_1^{\,2} - R_2^{\,2} + k^2}{2k} \quad \text{and} \quad y_0 = \sqrt{R_1^{\,2} - x_0^{\,2}} \quad . \tag{2.11}$$

$$x_0 = \frac{R_1^{\,2} - R_2^{\,2} - k^2}{2k} \quad \text{and} \quad y_0 = \sqrt{R_1^{\,2} - x_0^{\,2}} \quad . \tag{2.12}$$

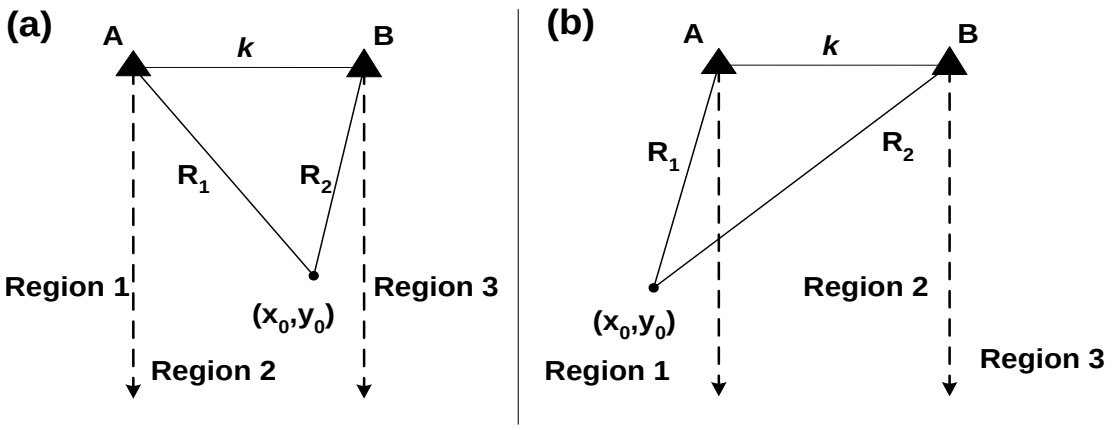

Figure 2.5: Determination of target localization for (a) Acute angle case; (b) Obtuse angle case.

2.5 Methodology

The synthesized system is based on SFCW radar which consists of two antennas placed at two positions A and B and is capable to collect the frequency domain data at these points. The reference data is subtracted from the data collected in the frequency domain after transforming them into spatial domain and thus gives rise to the target location peak in range profile. Although this target peak is tardy by some extent due to antenna system delay and advanced due to target curvature [Gaikwad *et al.* (2011)]. These distances are adjusted in the final calculated ranges. Once the target distance from the antenna A and B is obtained, the Euclidian distance formula is used to estimate the target location coordinate while k is the distance between two antennas and the coordinate of antenna A and B is assumed at (0, 0) and (*k*, 0), respectively. If the target location is outside the span of antenna joining baseline length *k* then it comes under obtuse angle case, i.e., subregions 1 and 3 else it lies under acute angle subregion 2. Depending upon either of these cases, the related expression pair mentioned in (2.11) or (2.12) is used to evaluate the coordinates of the object. By adjusting the antenna separation '*k*', target located in any shape within the CROS, can be localized but for ease of experimental demonstration,

rectangular region is selected. The complete processing methodology is given as the flowchart (Figure 2.6).

The acute angle or the obtuse angle case can be determined by using the algorithm provided in Figure. 2.7. In practical scenario for longer coverage applications, directional antennas are used which increases the system range. However, using the proper source of higher energy and using antenna of wider beamwidth, entire room monitoring could be covered but for checking the efficiency of the two antenna-based localization system we fix the antenna as shown in Figure 2.4 with rotation provision on their phase centre for collecting the data in entire rooms. In this study, a cylindrical target of 30 cm diameter is placed in a room of size 350 x 240 cm^2. For the given system, two types of capabilities have been investigated. The first one is spatial coverage on the available surface area of the rectangular room while the second one is through the wall localization, which makes the system more practical.

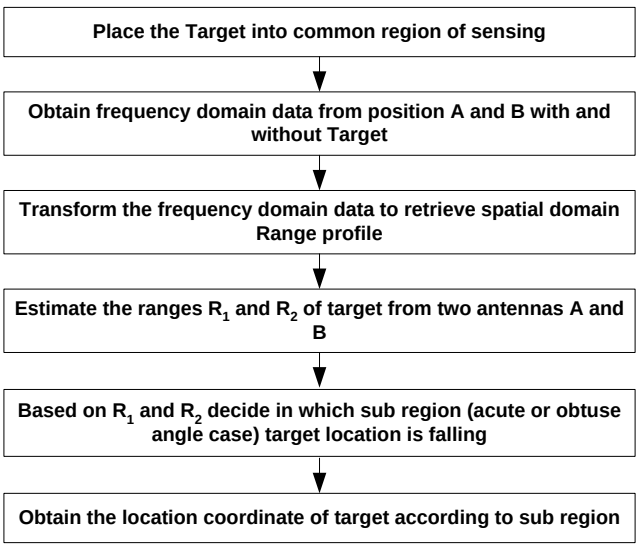

Figure 2.6: Flowchart of the processing methodology involved in the target localization.

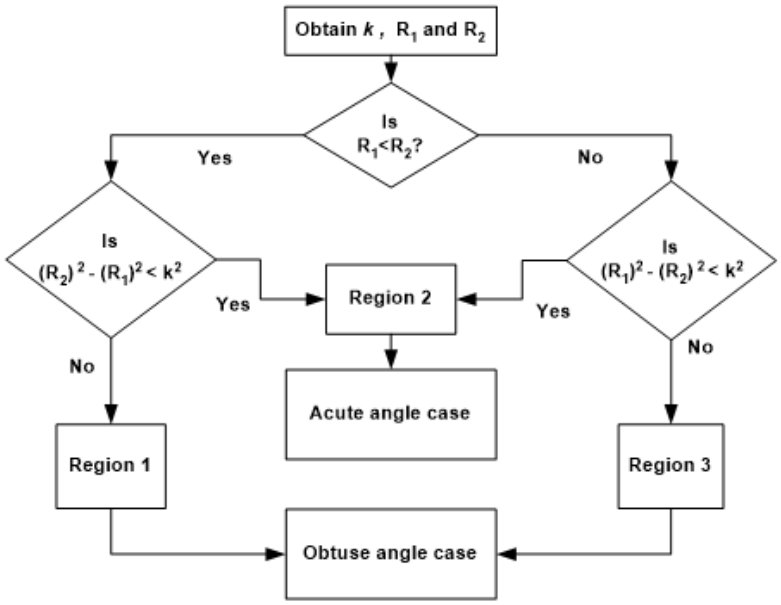

Figure 2.7: Algorithm for decision making for a subregion within the CROS.

2.5.1 Case A: Spatial Area Coverage Capability

To check the spatial coverage accuracy, data are collected for different target positions as shown in Figure 2.8(a). The coordinate of the measurement system lies on the line joining the two antennas as x-axis with antenna A placed at the origin (0, 0) while antenna B at the position (150, 0). A rectangular area is selected with corner coordinates (0, 75), (150, 75), (0, 325), and (150, 325; all units in cm) and this selected area is divided into a number of grids each of 50 cm length and 25 cm width. The target is placed at 35 points of the crossing of gridlines as shown in Figure 2.8(a). The A-scan is performed from the two antennas mounted on positions A and B to get the range estimation of the target.

2.5.2 Case B: Through the Wall Localization Capability

In this part of study, two plywood walls having different thickness of 1.1 and 2.2 cm are introduced alternatively within the CROS between the target and the localization system. This is illustrated in Figure 2.8(b) where the black dots represent the positions

in which the target is placed and the wall is represented by the red thick line. The data collection procedure is invariant to the previous case.

2.6 Results and Discussion

The target is placed on each of the nodes of the grid lines of the rectangle forming a matrix of 7x5 nodes as illustrated in Figure 2.8 (a). Each node is separated by 25 cm in *x*-direction while by 50 cm in *y*-direction. The range profile for (3, 2) grid position of the target, together with the reference range profiles generated from the data captured with antenna A are shown in Figure 2.9(a). Simultaneously, in Figure 2.9(a), the reference scan is also considered for the same grid position in absence of the target. Several peaks are observed at the same distance from the antenna A in the range profiles in both the scans except the target peak (marked as blue line in Figure 2.9(a)).

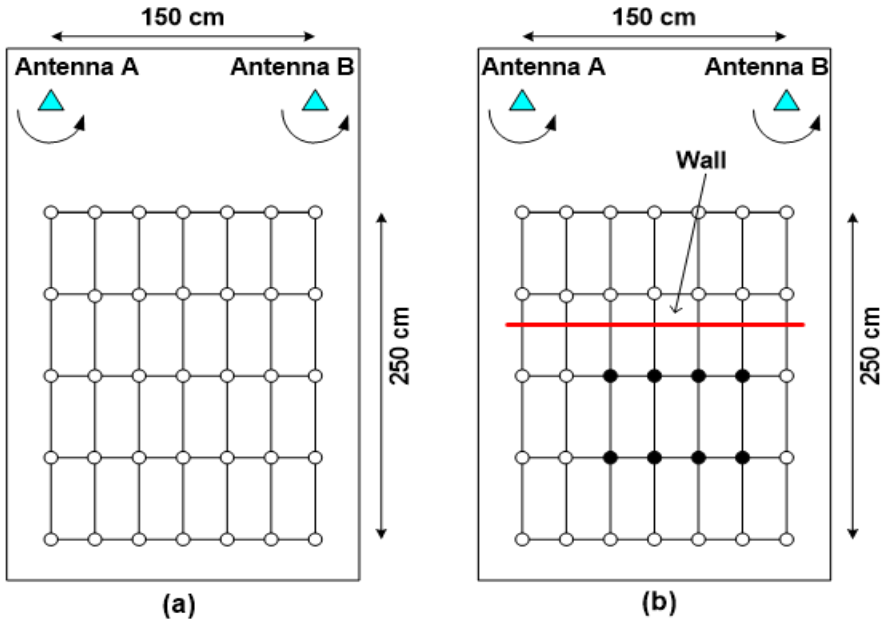

Figure 2.8: Target localization of the object using two antenna systems for (a) Free space and; (b) Through the wall environments.

All these peaks are originated due to some nearby scaterers or some system generated reflections as in the downrange directions from z = 0 cm to few cm, some reflections take place due to impedance mismatch of the antenna and associated adapter.

The same procedure to detect the peak in presence of the target, using antenna B is also performed and shown in Figure 2.9(b). The subtraction of the two range profiles in each case provides the improved signal to clutter ratio; thus enabling to identify the target distance clearly in the downrange direction. The range of the target from antenna A and B is identified clearly and given in Figures 2.10(a) and 2.10(b), respectively, where the appearance of single peak is observed. This peak is associated with target distance. For target located on grid point (3,2) the obtained range values from antenna A and B, i.e., R_1 and R_2 are 179.10 cm and 216.42 cm, respectively, as observed in Figures 2.10(a) and 2.10(b).

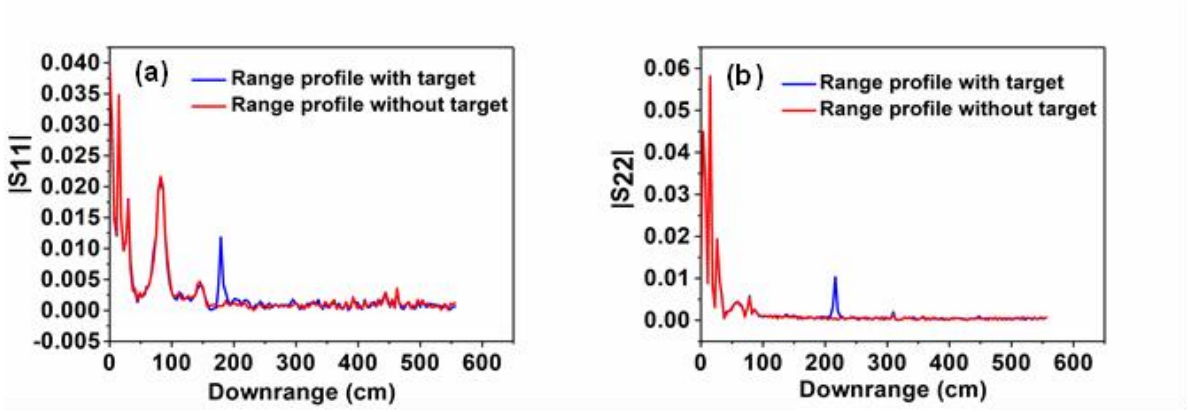

Figure 2.9: Generated range profiles for node position (3, 2) on the rectangular grid with and without target from (a) Antenna A and; (b) Antenna B.

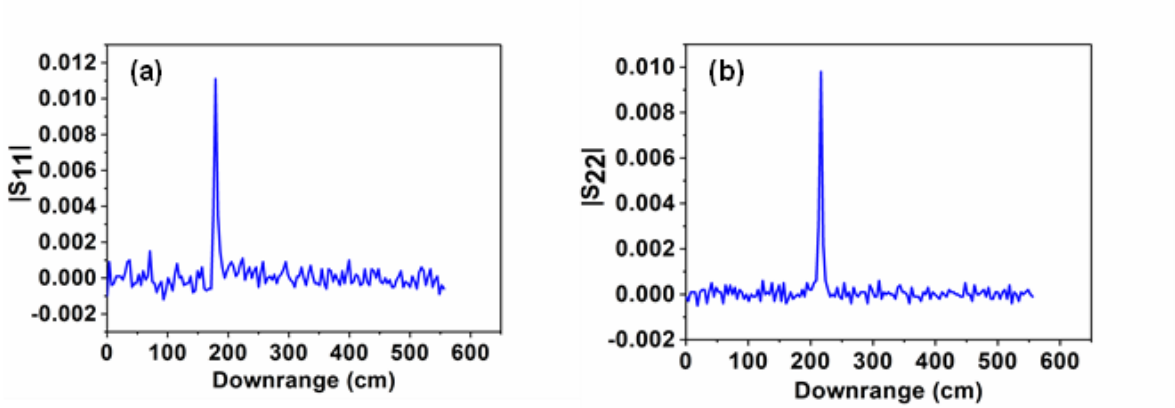

Figure 2.10: Actual target range generated for node position (3, 2) on the rectangular grid by subtraction of reference for (a) Antenna A and; (b) Antenna B.

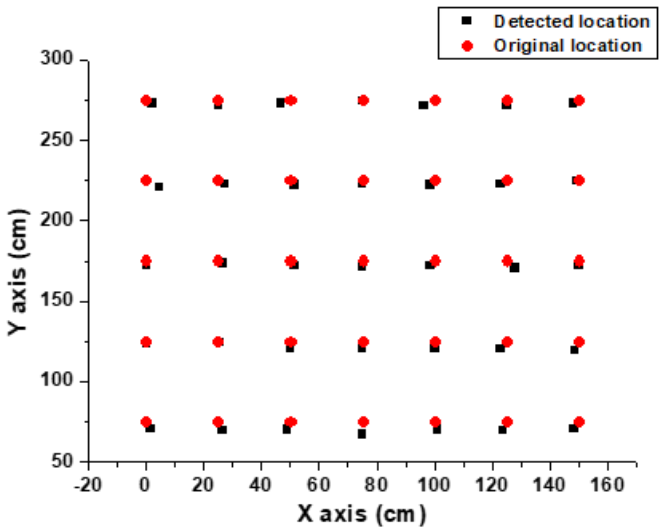

Figure 2.11: Detected location of the target using two antenna based system.

2.6.1 Case A Results

The actual positions of the target in Case A (as mentioned by grid points of Figure 2.8(a)) are represented by red circular dots while the detected locations of the target using the two antenna system are represented by black squared dots in Figure 2.11. It is observed that the actual and detected locations are differing with certain amount of radial distance error at each position of the target. The errors involved in each location of target are arranged according to the target location given as matrix A in equation (2.13). The columns of A are mutually separated by 25 cm while the rows of the same by 50 cm. Although two antenna system is capable to cover all possible three subregions 1, 2 and 3; however, due to access available for the total wall length, the antennas are mounted close to the two ends of the wall and all target placing positions comes under the case of acute angle, i.e., the target lying in subregion 2 of the CROS. The final coordinate detection depends on the range measurement of the target from known antennas positions, which are more prone to error due to system design limitations. Since the selected target is a cylinder, which is an extended target rather than a point scatterer whose surface curvature and height can also cause error in range

measurement, as depicted from Figure 2.11. The maximum radial distance error occurred at the target location of (75cm, 75cm) i.e. 4th location of the target placed and its value is 8.03 cm which is less than the objects radius, i.e., 15 cm.

$$A = \begin{pmatrix} 2.84 & 3.09 & 4.05 & 0.77 & 5.17 & 3.09 & 2.84 \\ 6.43 & 3.18 & 3.18 & 1.71 & 3.18 & 3.18 & 1.19 \\ 3.20 & 2.03 & 3.53 & 3.92 & 3.53 & 5.47 & 3.20 \\ 1.99 & 1.23 & 4.35 & 4.66 & 4.35 & 5.39 & 5.88 \\ 4.75 & 5.71 & 4.94 & 8.03 & 4.94 & 5.71 & 4.75 \end{pmatrix} . \quad (2.13)$$

2.6.2 Case B Results

In order to check through the wall localization capability of case B, the data are collected for 8 locations of the target as shown by black dots in Figure 2.8(b) by introducing a plywood wall of different thickness values of 1.1 cm and 2.2 cm. If the thickness of the wall is *'d'* then the wave emitted from the antenna has to travel twice through the wall material which offers a shift in target range measurement because it requires extra time $2d(\varepsilon_r - 1)/c$ to travel the round trip distance from antenna to target where $\varepsilon_r = 2.4$ for plywood [Chandra *et al.* (2008)]. This shifting in range is non-uniform for all the target positions as the travelled distance through the wall depends on the projection angle of the incident electromagnetic wave. But here global error correction is applied to compensate all the shifts due to the wall and projection angle and it is observed that the location detection error is within the acceptable limit for both the thicknesses of wall. Figure 2.12(a) shows the detected location of targets while the corrections needed to overcome the errors in the detected positions are listed as matrix B shown in equation (2.14) for the wall thickness of 1.1 cm. A plot of desired correction with respect to the positions is also given in Figure 2.12(b) and the maximum value of error occurs at the 3rd position with a value of 5.10 cm as evident from Figure 2.12(b) and matrix B given by equation (2.7). The measured ranges are influenced by the wall

material and after application of a common wall correction for each actual position of the target, the detected locations are shown in Figure 2.13(a) with the desired correction vs. position plot provided in Figure 2.13(b). If we look either at the correction matrix or the correction variation with respect to position graph after wall correction the error value gets improved and its maximum value occurs at 3rd target position with its improved value of 4.79 cm as seen from Figure 2.13 (b) and matrix C of equation (2.15).

$$B = \begin{pmatrix} 3.18 & 3.18 & 1.71 & 3.18 \\ 2.03 & 3.53 & 5.10 & 3.53 \end{pmatrix} \quad . \tag{2.14}$$

$$C = \begin{pmatrix} 2.24 & 2.10 & 0.50 & 2.10 \\ 1.16 & 2.36 & 4.79 & 2.36 \end{pmatrix} \quad . \tag{2.15}$$

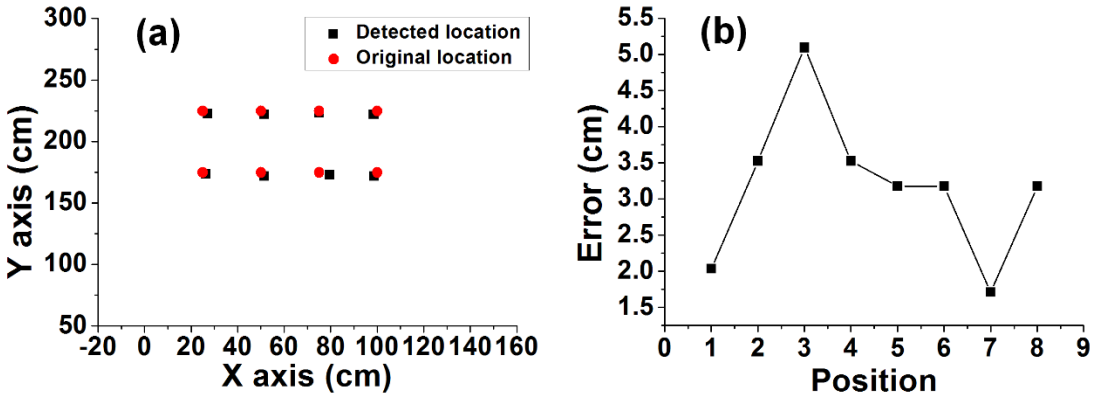

Figure 2.12: (a) Determination of positions of the target without wall correction; (b) Correction involved to eliminate the positional error for a 1.1 cm thick wall.

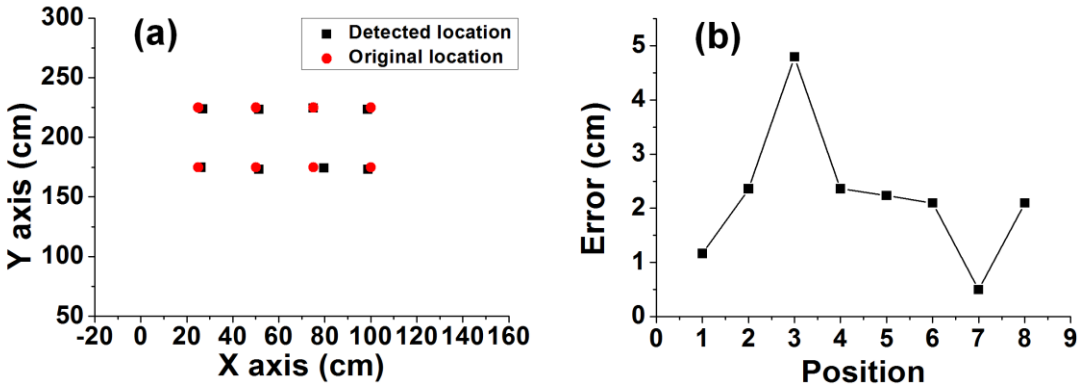

Figure 2.13: (a) Determination of positions of the target with wall correction; (b) Correction involved to eliminate the positional error for a 1.1 cm thick wall.

Similarly, for a wall of thickness 2.2 cm, the detected locations of the object are shown in Figure 2.14 (a). The errors in detected locations are illustrated in Figure 2.14(b) and tabulated in form of correction matrix D that must be incorporated for detection of actual location as mentioned in equation (2.16). It is evident from both Figure 2.14(b) and matrix D that the maximum error occurs in 6^{th} position indicated as 2^{nd} column of 1^{st} row. By incorporation of common wall correction in all the target ranges obtained from the antennas A and B, the required correction introduced in each measurement involving location estimate gets reduced as given in Figure 2.15(a), Figure 2.15(b) and matrix E of equation (2.17).

$$D = \begin{pmatrix} 3.18 & 7.20 & 1.71 & 6.87 \\ 2.03 & 4.02 & 5.10 & 4.02 \end{pmatrix} \quad . \tag{2.16}$$

$$E = \begin{pmatrix} 2.01 & 7.18 & 0.13 & 5.85 \\ 1.06 & 3.81 & 4.76 & 3.81 \end{pmatrix} \quad . \tag{2.17}$$

Due to the finite dimension of the object under consideration, the true estimate can be calculated if the detection lies within the width of the object failing which it gives rise to

a false indication [Kocur *et al.* (2013)]. In the present case, the target is a cylinder of diameter 30 cm and the maximum absolute error from the point of placement is calculated as 8.03 cm amidst all cases. The maximum error detected in location of the object thereby lies within the true estimation criteria assuring that all detected locations will satisfy the true estimate criterion; resulting in 100% true estimate in all the cases while the joining intersection of ellipse (JIEM) based detection scheme provides 88% true estimate as its best possible case [Kocur *et al.* (2013)].

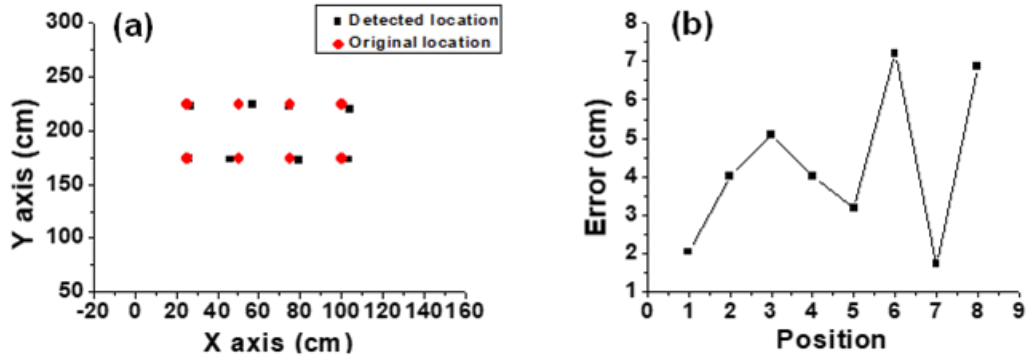

Figure 2.14: (a) Determination of positions of the target without wall correction; (b) Correction involved to eliminate the positional error for a 2.2 cm thick wall.

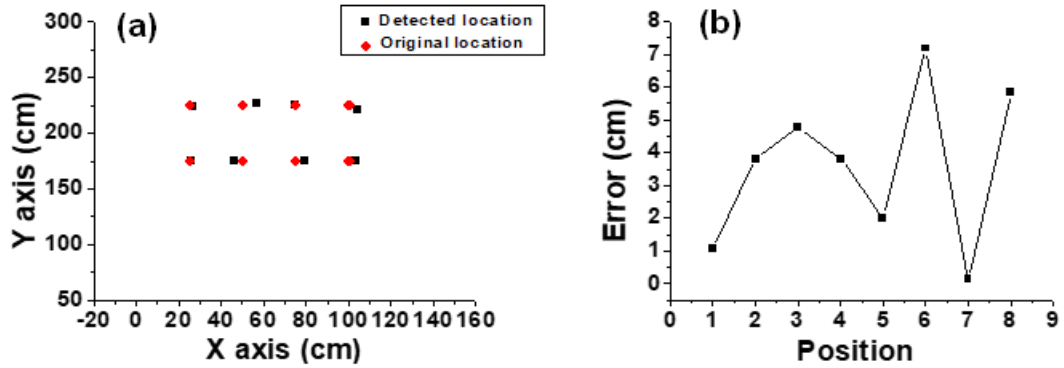

Figure 2.15: (a) Determination of positions of the target with wall correction; (b) Correction involved to eliminate the positional error for a 2.2 cm thick wall.

2.7 Conclusions

A two antenna based localization system working on the principle of SFCW radar was investigated to locate a target placed anywhere inside a rectangular region. The practical concern of target localization was analyzed as the common region of sensing (CROS) and possible subregions within the CROS during the implementation of such (two antenna based localization) system. The object location was determined in simple Cartesian coordinate defined with respect to the two antennas of the system. The experimental data for the free space and through the wall localization were collected and the correction matrices were subsequently generated. Applying the generated correction factor on the obtained object location, the precise location for each of the object was determined. The proposed scheme involves 100% true estimate in determining the object location compared to the reported true estimate.

The proposed low cost simple two antennas based SFCW radar target localization system involves direct solving the CROS-dependent localization relations instead of using any type of conventional optimization or estimation techniques; thereby reducing the complexity and producing the higher accuracy. Easier reference definition and the use of less number of antenna with flexible separation facilitates the ease of handling.